Optical response of C_{60} thin films and solutions

J. Hora, P. Pánek, K. Navrátil, B. Handlířová, and J. Humlíček

Department of Solid State Physics, Faculty of Science, Masaryk University, Kotlářská 2, 611 37 Brno, Czech Republic

H. Sitter and D. Stifter

Institut für Experimentalphysik, Johannes Kepler Universität Linz, A-4040 Linz, Austria

(Received 4 October 1995)

We report the optical spectra of C_{60} epitaxial films on mica with various thicknesses in the energy range from 1.4 eV to 6 eV, and for temperatures from 13 K to 300 K. The transmittance of toluene, hexane, and heptane solutions of known concentrations has also been studied; a significant shift of the absorption bands in these solvents has been found. We fitted our spectra with Gauss-Lorentz (GL) line shapes to determine the energy positions, oscillator strengths, and widths of individual transitions. It has been found that the GL profiles excellently approximate the optical response. We compare the dielectric function of solid and molecular C_{60} in detail, with special attention paid to the assignment of the forbidden and the lowest allowed transitions. [S0163-1829(96)01328-8]

I. INTRODUCTION

Fullerenes, and their crystalline form, fullerites, have attracted much attention in recent years due to their unusual properties. The interest is mainly focused on C_{60}, which has the highest molecular symmetry.[1] Solid C_{60} has a face-centered cubic crystal structure above $T_c = 257$ K, and below T_c, the fcc phase is transformed into a simple cubic lattice.[2] The electronic structure of this material has been investigated in detail by spectroscopic techniques including optical absorption,[3,4] ellipsometry,[5,6] Raman scattering,[7] photoemission and inverse photoemission,[8] electron energy-loss spectroscopy,[9] and in a number of theoretical studies.[10–14]

The optical measurements show three strong absorption bands in the 3–6 eV region. The band positions reported by various authors are in agreement within about 20 meV. The theoretical studies of the molecular structure indicate that this energy range is dominated by $\pi \rightarrow \pi^*$-like excitations, similar to the transitions in aromatic molecules.[10] The absorption edge is observed at 1.8–1.9 eV.[3,5] Because of the weak intermolecular interaction, the spectra of molecular and solid C_{60} are quite similar. There is also a fair agreement between experimental results and theoretical calculations concerning the transition energies; the differences are typically less than about 300 meV. However, a detailed assignment of the observed transitions is still under discussion.

In this paper, we investigate the optical response of solid C_{60} at various temperatures; moreover, we have studied the transmittance spectra of toluene, hexane, and heptane solutions of known concentrations. We analyze in detail the spectral line shapes of both solid and solutions. Thus we are able to compare the strength of absorption per molecule, and the positions and broadenings of the absorption bands in the crystalline and molecular form. We aim mainly at the lowest allowed and forbidden transitions; the knowledge of the temperature dependence as well as the comparison of C_{60}-toluene and C_{60}-hexane solutions has been found to provide useful guidelines.

The C_{60} molecule exhibits icosahedral symmetry; therefore the energy levels in the molecule are classified by the irreducible representations of the group I_h.[15] Because of the similarity of the electronic structure of the isolated C_{60} molecule and solid C_{60}, we classify the energy bands of the latter also by the irreducible representations of the group I_h.

II. EXPERIMENT

Four epitaxial layers of C_{60} with the nominal thicknesses of 140 nm, 190 nm, 340 nm, and 590 nm were grown on mica. The actual thicknesses obtained from the fit of the interference-dominated reflectance spectra in the near-infrared region were 162 nm, 185 nm, 367 nm, and 612 nm, with uncertainty less than 5 nm. The applied growth technique was hot wall epitaxy (HWE), since it has been shown that thin films of high crystalline quality can be prepared using this method.[16] A detailed description of the HWE system and the growth procedure can be found in Ref. 16. The substrate temperature was about 160 °C, the growth rate about 0.4 Å s^{-1}.

Near-normal incidence reflectivity of all samples was obtained at room temperature in the energy range 1.4–6.0 eV using a double beam spectrometer. Reflectance spectra of the 612 nm sample were also measured at low temperatures in the energy range 2.2–4.5 eV, and the measurements of the 185 nm sample were performed in the vicinity of the absorption edge (1.5–2.7 eV). The low temperature spectra were measured in a closed-cycle helium cryostat using a xenon arc lamp, a single grating monochromator, and a photomultiplier as a detector. We also performed ellipsometric measurements in the energy range 2.0–3.4 eV with a rotating analyzer ellipsometer.

For the solutions, a known volume of solid C_{60} from the mica-supported films was dissolved in toluene, as well as in hexane and in heptane. The transmittances of the solutions with respect to the pure solvent were obtained in the energy range 1.9–5.6 eV using 10 mm cells. All spectra were mea-

sured with a spectral resolution of 0.5 nm (1–15 meV). The accuracy of the temperature determination was better than 3 K.

III. RESULTS AND DISCUSSION

A. Solid C_{60}

In the low energy region, the optical spectra of all samples exhibit interference effects due to the multiple reflections within the C_{60} film. In order to establish the region, in which the absorption is strong enough to suppress the reflection from the back surface of the film, ellipsometric measurements of the thickest sample (612 nm) were performed and subsequently analyzed with a two-phase (ambient-bulk C_{60}) model. We have obtained an excellent agreement between the measured reflectivity and the reflectivity calculated from the ellipsometric data for energies above 2.35 eV. Consequently, the C_{60} film with the thickness of 612 nm is equivalent to the bulk material for photon energies above 2.35 eV. Comparing the reflectivity of the remaining samples with the reflectivity of the thickest film, we have also established the regions without the interference effect for the thinner films. The ranges start from 2.7 eV, 3.3 eV, and 3.4 eV for the film thicknesses of 367 nm, 185 nm, and 162 nm, respectively.

At first we tried to model the ellipsometric and reflectance data using a set of Lorentzian oscillators[4,5] for the complex dielectric function $\varepsilon = \varepsilon_1 + i\varepsilon_2$. However, unless the number of resonances is rather high, in which case the cross correlations of the fitted parameters prevent a reliable identification of the individual components, systematic discrepancies are observed. The measured spectral shapes of the absorptive part ε_2 exhibit distinctly flatter maxima compared to the model Lorentzian profiles. We therefore modified the model profiles by convolution with Gaussian profiles. The dielectric function is represented by the following sum of Gauss-Lorentz (GL) profiles:

$$\varepsilon(E) = \varepsilon_\infty + \sum_{j=1}^{n} \frac{S_j E_j^2}{\Gamma_{Gj}\sqrt{2\pi}} \int_{-\infty}^{\infty} \frac{e^{-(E_j-x)^2/2\Gamma_{Gj}^2}}{x^2 - E^2 - iE\Gamma_{Lj}} dx, \quad (1)$$

where ε_∞ is a constant, E_j denotes the oscillator positions, S_j the strengths, and Γ_{Lj} and Γ_{Gj} the Lorentzian and Gaussian widths, respectively. The real and imaginary parts obey the Kramers-Kronig relations and can be computed efficiently using the complex probability function.[17] The Lorentzian oscillators result in the limiting case of $\Gamma_G \to 0$. The nonzero Gaussian widths substantially improve the quality of the fit. The minimum number of GL profiles necessary to fit the spectra within the noise is 10. In fitting the spectra, we have assumed $\varepsilon_\infty = 1$. The contribution of the higher absorption bands has been represented by a single narrow peak located at 10 eV; its oscillator strength has been found to be about 1.56.

The three strongest absorption bands exhibit a pronounced doublet structure with the components of comparable strengths. The remaining four bands are rather weak, as shown for the absorptive part of the dielectric function in Fig. 1. The measured and best-fit reflectance spectra of the thickest film are plotted in the inset of Fig. 1. The sharp divergence below 2.35 eV, which was excluded from the fit,
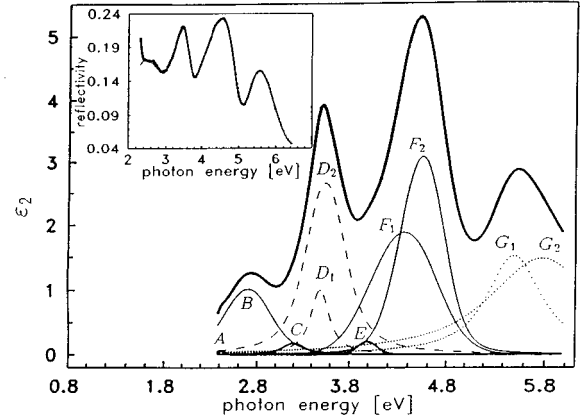

FIG. 1. The imaginary part of the dielectric function of solid C_{60} and the contributions of the individual Gauss-Lorentz bands. Inset: Measured reflectivity of the 612 nm film (crosses), and the best-fit of reflectivity by GL profiles (solid line).

is due to the multiple reflections within the film. The best-fit parameters of the GL profiles at room temperature are listed in Table I. The model enables us to determine the energy positions of the absorption bands with precision better than 10 meV. The error margins of the parameters have been estimated from the sample-to-sample differences, which are slightly larger than the uncertainty due to the errors in the optical measurements.

The response functions reported in Ref. 5 give a similar shape, but the absolute values of the reflectivity are about 4% lower; on the other hand, the reflectivity calculated from optical constants from Ref. 18 is about 6% higher. Our model of the GL profiles requires only ten absorption bands compared with 16 pure Lorentzians in Ref. 5 for the same spectral range. The low number of Lorentzian profiles used in Ref. 4 leads to errors significantly above the experimental uncertainty.

We attempted fitting the spectra at various temperatures with GL profiles by allowing variations of all of the adjustable parameters of Eq. (1), i.e., S_j, E_j, Γ_{Lj}, and Γ_{Gj}. However, strong correlations of the Gaussian and Lorentzian broadenings led to rather large error margins for the linewidths. Since the Gaussian widths were apparently independent of temperature, we then fixed them at the values averaged from the spectra for all temperatures, and fitted Γ_L only. The only exception was the band F_1, which exhibits large Gaussian and negligible Lorentzian widths. This band probably consists of several overlapping subbands. In this case, we fixed the Lorentzian broadening at 0.01 eV and fitted Γ_G. With decreasing temperature, we observe a pronounced decrease of the Lorentzian widths as seen in Fig. 2 which summarizes the temperature dependences of the oscillator strengths, transition energies, and Lorentzian and Gaussian widths. The broadening of the absorption bands described by the Gaussian and Lorentzian widths can have several origins. In addition to the finite temperature-dependent lifetime of excited states in the otherwise unperturbed molecules, the broadening can be also caused by the band dispersions and/or lattice and bond length fluctuations.

In the transparent (low energy) region, we have taken the reflectivity spectra from both the front and back faces of the
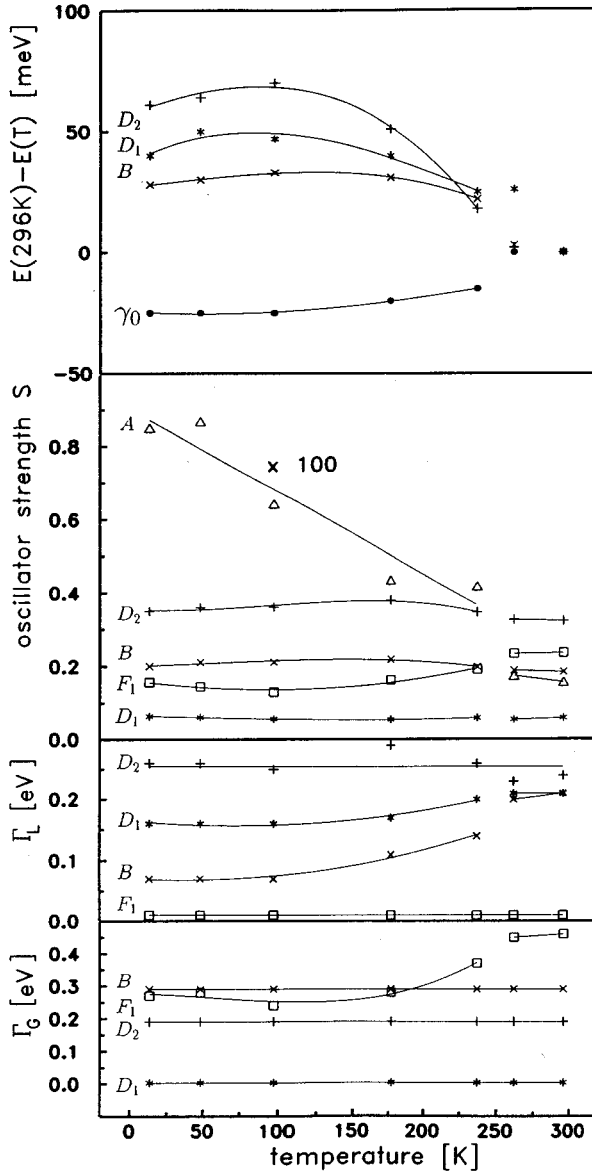
FIG. 2. The temperature dependences of the transition energies, the oscillator strengths, and the Lorentzian and Gaussian widths for selected bands of solid C_{60}. The oscillator strength of the A band is multiplied by 100. The lines are guides to the eye.

C_{60}/mica samples. After correcting for the reflections of the mica-ambient interface, we observe differences less than 0.1% between both spectra below $E_g = 1.765 \pm 0.015$ eV. This indicates a negligible absorption ($\varepsilon_2 \leqslant 0.002$) of the C_{60} film in this energy range. The measured reflectivity of the thickest (612 nm) film, after having been corrected for the mica-air reflections (i.e., for the three-phase air-C_{60}-mica structure), is plotted in Fig. 3. This spectrum was fitted below 1.7 eV assuming zero absorption of the film. The best-fit reflectivity is also shown, including its extrapolation above the fitted range. The dispersion of the refractive index n of the C_{60} film follows a simple quadratic dependence, $n = n_0 + bE^2$, with $n_0 = 2.02$ and $b = 0.05$ eV^{-2}. Let us note that the constant value of n_0 summarizes the strength of the electronic transitions; the result obtained from the interference effects in the transparent region is in very good
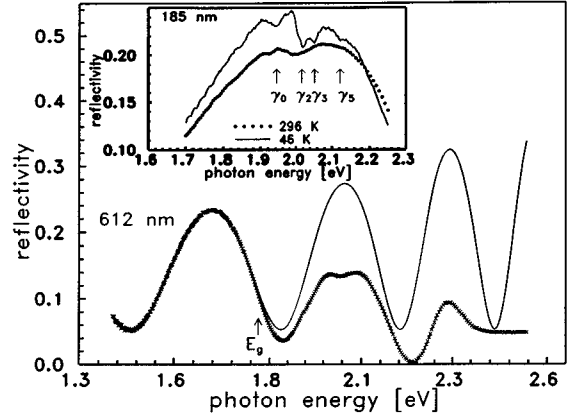

FIG. 3. The reflectance spectra of a 612 nm film at room temperature corrected for the mica-air reflections (crosses); the best-fit reflectance in the nonabsorbing region below 1.7 eV and its extrapolation above 1.7 eV (solid line). Inset: The reflectivity of the 185 nm sample at 296 K (bullets) and at 46 K (solid line). The arrows indicate the peak positions at 46 K.

agreement with the value of 2.04 resulting from the sum of the GL bands of Table I. The extrapolated refractive index of the film increases towards higher energy while the absorption remains zero, which produces the continuing interference pattern of increasing amplitude and shrinking period. The actual reflectance starts to deviate gradually from this extrapolation at the above value of $E_g \approx 1.77$ eV, shown by the arrow in Fig. 3. The difference is due to the absorption in the film, and related deviations of the actual refractive index from the extrapolated values. At the interference minima, the reflectivity is lowered by the absorption, while being independent, to the first order, on the film refractive index. Using the data of Fig. 3, we are able to estimate the slope of the smooth and weak onset of the absorption starting at E_g; the slope of ε_2 is 0.5 ± 0.2 eV^{-1}. The fine structure superposed on the smooth background becomes much sharper at low temperatures, as shown in the inset of Fig. 3. We label here the four resolved structures according to the corresponding features of the solution spectra described in the next subsection.

B. C_{60} molecules in solutions

For the transmittance measurements, the thinnest C_{60} film (amounting to 3.2×10^{-5} g) was completely dissolved in 2 ml of toluene. The concentration of C_{60} molecules in the solution was 6.5×10^{15} cm^{-3}. Assuming a constant refractive index n_0 of 1.50 for toluene,[19] we can readily express the complex dielectric function ε_s of the solution in terms of the measured relative transmittance T_d in the cell of the length d:

$$\varepsilon_s = n_0^2 - i \frac{1}{2\pi} \frac{n_0 \lambda}{d} \ln(T_d). \qquad (2)$$

Further, we approximate the optical response of the solution via the Maxwell-Garnett effective medium[20] with two com-

TABLE I. The best-fit GL profiles parameters from the reflectance spectra of solid C$_{60}$ and from the ε_2 spectra of the C$_{60}$-hexane solution, at room temperature.

Band code	Solid C$_{60}$				C$_{60}$ molecules				Assignment
	E (eV)	S	Γ_L (eV)	Γ_G (eV)	E (eV)	S	Γ_L (eV)	Γ_G (eV)	
A	2.41(4)	0.002(1)	0.01	0.05					
B	2.70(1)	0.174(5)	0.20(4)	0.29(1)					$\left.\right\} h_u \to t_{1g}$
C	3.2(1)	0.015(7)	0.20(7)	0.10(5)					
D_1	3.489(4)	0.070(8)	0.24(2)	0.003	3.58(1)	0.08(1)	0.01(1)	0.280(4)	$\left.\right\} h_g, g_g \to t_{1u}$
D_2	3.541(2)	0.327(8)	0.30(6)	0.19(5)	3.732(4)	0.09(1)	0.09(2)	0.085(7)	
E	3.99(1)	0.009(2)	0.04(8)	0.13(5)	4.21(6)	0.04(1)	0.02	0.21(5)	
F_1	4.36(1)	0.231(3)	0.01	0.47(8)	4.60(2)	0.46(8)	0.21(1)	0.21(1)	$h_u \to h_g$
F_2	4.546(4)	0.266(5)	0.10(2)	0.29(2)					
G_1	5.500(6)	0.179(7)	0.65(2)	0.005	5.437(4)	0.019(3)	0.01	0.11(1)	$\left.\right\} h_g, g_g \to t_{2u}$
G_2	5.77(1)	0.32(2)	1.25(3)	0.01	5.73(1)	0.33(3)	0.66(1)	0.001	

ponents, i.e., the host solvent with the constant dielectric function n_0^2, and the molecular C$_{60}$ with a complex dielectric function ε_m:

$$f \frac{\varepsilon_m - n_0^2}{\varepsilon_m + 2n_0^2} = \frac{\varepsilon_s - n_0^2}{\varepsilon_s + 2n_0^2}, \tag{3}$$

where f is the volume fraction of C$_{60}$ in the solution. Using this formula, we obtain the dielectric function ε_m of an idealized species of noninteracting C$_{60}$ molecules having the same density as crystalline C$_{60}$. Because of the cubic structure of the latter,[21] the local field enhancement is expected to be close to that of the solution, where the surroundings of each C$_{60}$ molecule are nearly spherical.[22]

In the less polar solvents, hexane and heptane, the dissolution of the thicker films has been found to stop after dissolving about 200 nm, leaving an apparently inhomogeneous C$_{60}$ film covered by a protective layer. In order to fix the value of the concentration of C$_{60}$ molecules in these solutions, we have assumed the same oscillator strength of the D_2 band at 3.7 eV in all of the solvents. The knowledge of the concentration has enabled us to determine the ε_2 spectra on an absolute scale, see Fig. 4. The lower magnitude of the D_2 peak values of the hexane solution are due to the lower refractive index of hexane (~ 1.38 compared with ~ 1.50 for toluene[19]). Our hexane solution spectra virtually coincide with the results of Leach et al.;[3] we have used their high energy tail to expand our spectra to 6 eV. We have excluded the weak structures near 4.4 eV and 4.5 eV from the subsequent analysis, because it is not clear if they are intrinsic to C$_{60}$. The reason is the absorption structure of hexane itself in this energy range, peaking at 4.39 eV and 4.54 eV; these bands could be enhanced by the solute-solvent interaction. This conclusion is also supported by the difference between the hexane and heptane spectra.

The asymmetric overlapping bands of ε_s can be roughly fitted using ε_m, represented by three pairs of Lorentzian oscillators. However, a significantly better fit results by using the GL line shapes; the best-fit parameters listed in Table I produce agreement within the noise level.

The imaginary part of ε_m, and its decomposition into the individual GL bands, is plotted in Fig. 5; displayed here is also the ε_2 spectrum of the solid from Fig. 1. We can see that the major modifications of the response of crystalline C$_{60}$ compared to the noninteracting molecules consist of (i) the appearance of the strong band B at ~ 2.7 eV; (ii) the redshift of the $D_{1,2}$, E, and $F_{1,2}$ bands by ~ 0.05 to ~ 0.2 eV; (iii) nearly doubling the widths, with the exception of the E and the lower component of the D bands; the full widths at half maximum computed from the parameters of Table I are listed in Table II; and (iv) a moderate redistribution of the oscillator strengths between the three leading bands and within the components; the increase of the total oscillator strength between 3 eV and 6 eV is about 40%.

The large width of the D_1 band in the solutions is probably caused by overlapping with the set of B and B' bands on its low energy wing. This multicomponent fine structure has been ignored in constructing the spectra of Fig. 5. However, it is strongly enhanced by computing the second derivative of ε_2 shown in the inset of Fig. 4. The spectra of the toluene solution have to be rigidly shifted by 23 meV to-
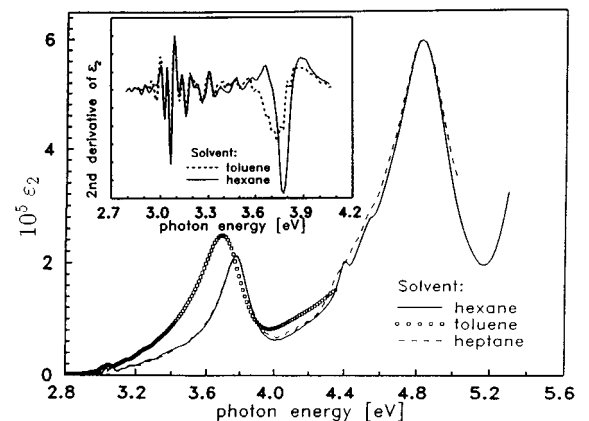

FIG. 4. The ε_2 spectra of C$_{60}$ solutions with the concentration of 6.5×10^{15} cm^{-3}. Inset: The second derivative of the C$_{60}$ solution ε_2 spectra (the C$_{60}$-toluene spectrum is shifted by 23 meV towards higher energies).
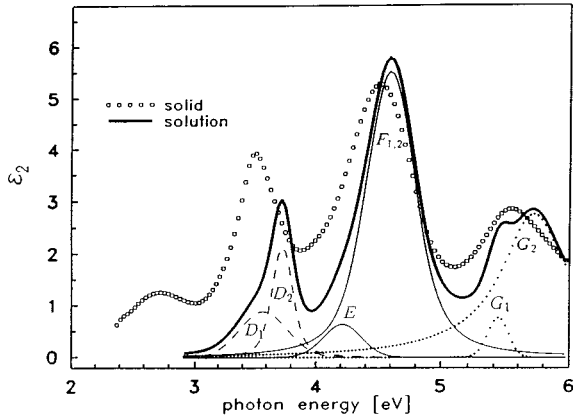
FIG. 5. The ε_2 spectrum of solid C_{60} and the ε_2 spectrum of molecular C_{60} (with the same density as the solid state) and the contributions of the individual bands to ε_2 for the latter.

FIG. 6. The ε_2 spectra of C_{60} solutions with the same concentration as in Fig. 4.

wards higher energy to obtain a very good agreement of the B band fine-structure positions with the hexane solution. This energy shift is likely to be due to the field of the strongly polar toluene molecules.

The absorption edge of ε_m is located at 1.9 eV. The weak absorption bands above this energy exhibit a fine structure not seen on the scale of Fig. 4; they are plotted in Fig. 6. The positions of a number of resolved peaks are in good agreement (within $\sim$ 3 meV) with the results of Leach *et al.*[3] We have therefore taken over their notation order for the group of γ. From a series of peaks in the spectra of Ref. 3 near $\sim$2.9 eV, we resolved only two shoulders at 2.920 eV and 2.963 eV in the toluene solution.

The comparison of the fine-structure positions in the toluene and hexane solutions in the energy range 1.9–4.0 eV can help to distinguish the individual electronic transitions. According to the energy shift, we can form four separate groups of subbands which are labeled by γ, B, B', and D. The peak positions of the individual transitions are summarized in Table III. Let us note that the centers of the strong bands D, F, and G obtained from the fit significantly differ from the peak positions in the ε_2 spectra (Fig. 4) due to the mixing of the real and imaginary parts of the dielectric function ε_m in the Maxwell-Garnett formula [Eq. (3)]. For example, the peak position of the D_2 band (3.775 eV) is shifted from its center position (3.732 eV) by 43 meV.

Since our spectra are measured with the known concen-

trations, we also obtain the oscillator strengths. The strengths of the transitions B_0, B_1 at $\sim$3 eV are about 0.003, while the strengths of the individual bands of the $\gamma_0-\gamma_5$ family are only about 0.001. Several components of this fine structure with oscillator strengths about 0.002, which are rigidly shifted about 77 meV towards lower energies, are also resolved in our spectra of solid C_{60}; see Table III. The positions were extrapolated from the low temperature measurements, since they are nearly smeared out at room temperature; see Fig. 3. The oscillator strengths of the fine structures in solid seem to be slightly lower than those in solutions. The imaginary part of ε_m exhibits a nearly linear background below the lowest vibrational peak γ_0. Its strength is comparable with the background observed in the room temperature data of the films: the slope of $\sim$0.3 eV^{-1} is to be compared with the value of $\sim$0.5 eV^{-1} found in the preceding subsection. This indicates rather weak solid state effects in these lowest, dipole-forbidden transitions. The energy separation of the strongest γ_2 and γ_3 bands coincides with the splitting seen in the second harmonic spectra of Ref. 23.

C. Assignment of the energy levels

Our assignment of the electronic transitions given in Table IV is based on the calculated transition energies of Refs. 10, 11, and 13. The best agreement of the calculated gap positions with experimental results is provided by the tight-binding models.[11,13] Models based on local-density approximation (LDA) calculations[24,12] underestimate the gap; on the other hand, the quasiparticle approach of Ref. 14 significantly overestimates it. An overview of the energy levels and optical transitions discussed below is shown in Fig. 7.

We start with the assignment of the three leading GL bands D, $E+F$, and G, to the transitions $h_g, g_g \rightarrow t_{1u}$, $h_u \rightarrow h_g$, and $h_g, g_g \rightarrow t_{2u}$, respectively, which agrees with the assignment used in Ref. 5. The oscillator strengths of these dipole-allowed transitions are in reasonable agreement with the calculations of Ref. 11. The D band assigned to $h_g, g_g \rightarrow t_{1u}$ transitions has been found to be strongly reduced in doped films due to the filling of the lowest state in the conduction band derived from the t_{1u} molecular states.[25] The

TABLE II. Full width at half maximum of the main absorption bands of solid and molecular C_{60}.

Band code	FWHM (eV)	
	Solid C_{60}	C_{60} molecules
D_1	0.24	0.46
D_2	0.51	0.19
E	0.25	0.36
F_1	0.80	0.47
F_2	0.54	
G_1	0.65	0.20
G_2	1.26	0.66

TABLE III. Peak positions of the fine structure of the absorption bands in the energy range 1.9–4.0 eV.

Band code	C_{60} in hexane E_h (eV)	C_{60} in toluene E_t (eV)	Solid C_{60} E_s (eV)	Shift $E_h - E_t$ (meV)	Assignment
γ_0	1.995	1.985	1.918	10	$h_u \to t_{1u} + T_u, H_u, G_u$
γ_1	2.035	2.022		13	$(+H_g, A_g)$
γ_2	2.070	2.060	1.992	10	
γ_3	2.105	2.090	2.028	15	
γ_5	2.180	2.170	2.097	10	
B_0	3.035	3.012	2.70	23	$h_u \to t_{1g} + H_g(7)$
B_1	3.065	3.042		23	$h_u \to t_{1g} + H_g(6)$
B_2	3.123	3.100		23	$h_u \to t_{1g} + H_g(3)$
B_3	3.168	3.145		23	$h_u \to t_{1g} + H_g(1)$
B_4		3.203			
B_5		3.231			
B'_0	3.280	3.249		31	$h_u \to t_{1g} + H_g(8)$
B'_1	3.357	3.326		31	$h_u \to t_{1g} + H_g(5)$
B'_3	3.46				$h_u \to t_{1g} + H_g(1)$
D_2	3.775	3.695	3.539	80	$h_g, g_g \to t_{1u}$

molecular $F_{1,2}$ band, which originates from the $h_u \to h_g$ transition, is split into F_1 and F_2 bands in the solid. This is due to the splitting of the fivefold degenerate $h_u(h_g)$ levels to the threefold and twofold degenerate $t_u(t_g)$ and $e_u(e_g)$ levels, respectively.[26] The weak E band possibly also originates from the $h_u \to h_g$ transition.

The assignment of the two lowest transitions, $h_u \to t_{1u}$ and $h_u \to t_{1g}$, is more delicate. The $t_{1g} h_u^{-1}$ molecular state consists of electron-hole excited states with T_{1u}, T_{2u}, H_u, and G_u symmetry.[27] According to several calculations, the lowest allowed transition $h_u \to t_{1g}$ to the T_{1u} excited state should be located near 3 eV with an oscillator strength of about 3% of

that of the $h_g, g_g \to t_{1u}$ band at 3.5 eV;[11,10,28] the very small oscillator strength has been attributed to plasmon screening.[11] In addition to this allowed transition, phonon-induced transitions of comparable strengths[28] to the T_{2u}, H_u, and G_u excited states[27] should appear in the same energy region. The comparison of the energies and oscillator strengths of the B and D bands is essential for the following assignment of γ, B, B', and D subbands to the electronic transitions (see Table IV).

(i) γ, the group resulting from the forbidden molecular transition $h_u \to t_{1u}$. These transitions gain nonzero strength through the excitation of an appropriate odd-parity vibra-

TABLE IV. Room temperature transition energies and oscillator strengths obtained from the fit of the ε_2 spectra of C_{60}-hexane solution, and calculated transition energies (oscillator strengths). The parameters of the B_0 and B'_0 bands are a rough estimate based on the comparison with the D_2 band, assuming $\varepsilon_{2\max} \sim S/\Gamma$.

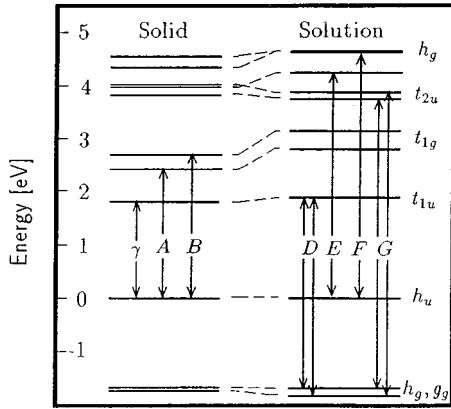| Band code	Transition energy E (eV)	Oscillator strength S	Assignment	Calculated transition energy (eV) (oscillator strength) Ref. 13	Ref. 11	Ref. 10
γ_0	1.995	0.001	$h_u \to t_{1u}$	2.1–2.8	>2.2	
B_0 B'_0	3.035 3.280	0.003 0.001	$h_u \to t_{1g}$	3.0	2.9	3.4
D_1 D_2	3.58 3.732	0.08 0.09	$h_g, g_g \to t_{1u}$	3.4	3.7(0.26)	4.06 4.38
E $F_{1,2}$	4.21 4.60	0.04 0.46	$h_u \to h_g$	4.79	4.7(0.46)	4.9 5.24
G_1 G_2	5.437 5.73	0.019 0.33	$h_g, g_g \to t_{2u}$	5.61 6.11 6.35	5.6(0.47) 6.1(0.52)	5.54 5.78 6.28

FIG. 7. The electronic energy levels in solid C_{60} and C_{60} dissolved in *n*-hexane.

tional mode[21] (Hertzberg-Teller coupling) and their upper electronic states can be influenced by Jahn-Teller dynamic distortions.[3]

(ii) B, B', the group resulting from the $h_u \rightarrow t_{1g}$ transition to the excited states with the T_{1u}, T_{2u}, H_u, and G_u symmetry. The transitions to T_{2u}, H_u, and G_u states gain strength due to the coupling to Herzberg-Teller active vibrational H_g modes[27] and can be associated with the fine structure $(B_0, B_1, \ldots, B'_0, B'_1, \ldots)$. The lowest allowed transition to the T_{1u} excited state is probably hidden under the low energy tail of the D_1 band and contributes to the background of the B and B' vibrational peaks. Consequently, the strength of this transition can be considerably higher than found in Refs. 11 and 28. The triply degenerate T_{1u} state should exhibit a Jahn-Teller effect;[3] therefore it can also contribute to the fine structure. Taking into account the frequencies of the Raman active H_g and A_g modes,[7] the assignment listed in Table III (in agreement with Yabana and Bertsch[27]) seems to be the most appropriate.

(iii) D_1, D_2, the group resulting from the second and third allowed transitions $h_g, g_g \rightarrow t_{1u}$. The energy separation of the $h_g \rightarrow t_{1u}$ and $g_g \rightarrow t_{1u}$ is beneath the accuracy of the theoretical studies.[11,12,25]

The D_2 band position is shifted from 3.732 eV in the solution to 3.543 eV in the solid, and the D_1 band position from 3.58 eV to 3.49 eV. We expect a similar shift of the B band, which originates from the $h_u \rightarrow t_{1g}$ transition. We can therefore assign this transition to the absorption band centered at 2.70 eV in solid C_{60}. The temperature dependence of the energy position and the oscillator strength support the assignment to the allowed transition resulting in the T_{1u} excited state. The decrease of the transition energy of the B band at low temperatures is similar to the D_1 and D_2 bands, which are due to the allowed $h_g, g_g \rightarrow t_{1u}$ transitions, while the temperature dependence of the forbidden transitions $\gamma_0, \gamma_1, \gamma_2, \ldots$ is considerably different, as is seen in Fig. 2. This different behavior seems to exclude the alternate $h_u \rightarrow t_{1u}$ origin of the B band at 2.70 eV.

The oscillator strengths of the B, D_1, and D_2 transitions are similar and slowly decreasing at higher temperatures in

contrast with the strength of band A, which is significantly lower, and rapidly increasing towards lower temperature. Therefore we assign the A band to the transitions to the H_u, G_u, or T_{2u} molecular states comprised in the $t_{1g}h_u^{-1}$ electron-hole excited state, which are parity forbidden in the isolated molecule. In the simple-cubic low temperature phase, these states split as follows: $G_u \rightarrow 2A_u + E_u + 4T_u$, $H_u \rightarrow A_u + 2E_u + 5T_u$, and $T_{2u} \rightarrow A_u + E_u + 3T_u$.[29] Consequently, the optically allowed transitions to the T_u states appear. At room temperature, when the molecules in the solid rotate rapidly, the effect of the crystal field is weak. The rotations are gradually frozen below 257 K,[30,31] increasing the influence of the crystal field and giving strength to the A band. Our direct observation of the increased absorption with decreasing temperature is in agreement with the resonant enhancement of Raman intensity.[29]

IV. CONCLUSION

We have investigated the optical response of epitaxial solid films and dissolved C_{60} by several optical techniques—reflectance, ellipsometry, and transmittance. The comparison of the ellipsometry and reflectivity separates the (thickness-dependent) regions influenced by multiple reflections in the C_{60} films. Our spectra reveal a smooth onset of absorption of the crystalline C_{60} at 1.765 eV, about 0.1 eV below the absorption edge of C_{60} molecules. The position of E_g is higher compared to the results of the LDA calculation (1.04 eV), but lower than the value of 2.15 eV obtained by the quasi-particle approach.[14]

Four separate groups of electronic transitions in the energy range 1.9–4.0 eV have been distinguished by comparison of the spectra of C_{60} dissolved in various solvents. The decompositions into the series of GL bands provides a suitable basis for *quantitative* comparison of the optical response of molecular and crystalline C_{60}. The oscillator strengths are in fair agreement with the values from several theoretical studies. We have found that a fairly low number of GL profiles excellently represents the dielectric function (ten for the solid and six for C_{60} dissolved in hexane). We have thus measured the energy shifts, redistribution of oscillator strengths, and changes of the bandwidths. In particular, the lowest, phonon-assisted electronic transitions are quite comparable in the crystalline and molecular forms of C_{60}. On the other hand, the bandwidths of the allowed transitions are approximately doubled in the solid.

In summary, we believe we have obtained a consistent picture of the optical transitions in C_{60}.

[1] W. Krätschmer, L. D. Lamb, K. Fostiropoulos, and D. R. Huffman, Nature **347**, 354 (1990).

[2] P. A. Heiney, J. Phys. Chem. Solids **53**, 1333 (1992).

[3] S. Leach, M. Vervloet, A. Desprès, E. Bréheret, J. P. Hare, T. J. Dennis, H. W. Kroto, R. Taylor, and D. R. M. Walton, Chem. Phys. **160**, 451 (1992).

[4] Ting Wang, J. M. Holden, A. M. Rao, Wen-Tse Lee, X. X. Bi, S. L. Ren, G. W. Lehman, G. T. Hager, and P. C. Eklund, Phys. Rev. B **45**, 14 396 (1992).

[5] M. K. Kelly, P. Etchegoin, D. Fuchs, W. Krätschmer, and K. Fostiropoulos, Phys. Rev. B **46**, 4963 (1992).

[6] S. L. Ren, Y. Wang, A. M. Rao, E. McRae, J. M. Holden, T. Hager, K. A. Wang, Wen-Tse Lee, H. F. Ni, J. Selegue, and P. C. Eklund, Appl. Phys. Lett. **59**, 2678 (1991).

[7] D. S. Bethune, G. Meijer, W. C. Tong, H. J. Rosen, W. G. Golden, H. Seki, C. A. Brown, and M. S. Derries, Chem. Phys. Lett. **170**, 167 (1990).

[8] J. L. Martins, N. Troullier, and J. H. Weaver, Chem. Phys. Lett. **180**, 457 (1991).

[9] G. Gensterblum, J. J. Pireaux, P. A. Thiry, R. Caudano, J. P. Vigneron, Ph. Lambin, A. A. Lucas, and W. Krätschmer, Phys. Rev. Lett. **67**, 2171 (1991).

[10] M. Braga, S. Larsson, A. Rosén, and A. Volosov, Astron. Astrophys. **245**, 232 (1991).

[11] G. F. Bertsch, A. Bulgac, D. Tománek, and Y. Wang, Phys. Rev. Lett. **67**, 2690 (1991).

[12] A. Oshiyama, S. Saito, Y. Miyamoto, and N. Hamada, J. Phys. Chem. Solids **53**, 1689 (1992).

[13] K. Harigaya and S. Abe, Phys. Rev. B **49**, 16 746 (1994).

[14] E. L. Shirley and S. G. Louie, Phys. Rev. Lett. **71**, 133 (1993); J. Phys. Chem. Solids **54**, 1767 (1993).

[15] F. Negri and G. Orlandi, Chem. Phys. Lett. **144**, 31 (1988).

[16] D. Stifter and H. Sitter, Appl. Phys. Lett. **66**, 679 (1995).

[17] J. Humlíček, E. Schmidt, L. Bočánek, R. Švehla, and K. Ploog, Phys. Rev. B **48**, 5241 (1993).

[18] P. Milani, M. Manfredini, G. Guizzetti, F. Marabelli, and M. Patrini, Solid State Commun. **20**, 639 (1994).

[19] *Optische Konstanten, Zahlenwerte und Funktionen aus Physik, Chemie, Astronomie, Geophysik, und Technik,* edited by K.-H. Hellwege and A. M. Hellwege, Landolt-Börnstein, Pt. 8 (Springer-Verlag, Berlin, 1962).

[20] G. A. Niklasson and C. G. Granqvist, J. Appl. Phys. **55**, 3382 (1984).

[21] M. S. Dresselhaus, G. Dresselhaus, and P. C. Eklund, J. Mater. Res. **8**, 2054 (1993).

[22] S. R. Nagel and T. A. Witten, Phys. Rev. B **11**, 1623 (1975).

[23] A.-M. Janner, B. Koopmans, H. T. Jonkman, and G. A. Sawatzky, in *Proceedings of the International Winterschool on Electronic Properties of Novel Materials: Physics and Chemistry of Fullerenes and Derivatives*, edited by H. Kuzmany, J. Fink, M. Mehring, and S. Roth (World Scientific Publishing, Singapore, 1995).

[24] Yong-Nian Xu, Ming-Zhu Huang, and W. Y. Ching, Phys. Rev. B **44**, 13 171 (1991).

[25] T. Pichler, M. Matus, J. Kürti, and H. Kuzmany, Solid State Commun. **81**, 859 (1992).

[26] N. Troullier and J. L. Martins, Phys. Rev. B **46**, 1754 (1992).

[27] K. Yabana and G. F. Bertsch, Chem. Phys. Lett. **197**, 32 (1992).

[28] M. I. Salkola, Phys. Rev. B **49**, 4407 (1994).

[29] V. G. Hadjiev, P. M. Rafailov, C. Thomsen, and M. K. Kelly (unpublished).

[30] R. Saito, G. Dresselhaus, and M. S. Dresselhaus, Phys. Rev. B **49**, 2143 (1994).

[31] P. J. Horoyski and M. L. W. Thewalt, Phys. Rev. B **48**, 11 446 (1993).